RSC Advances

PAPER

View Article Online
View Journal | View Issue

Cite this: *RSC Adv.*, 2015, **5**, 43750

Enhanced photoluminescence of pyrrolic-nitrogen enriched graphene quantum dots†

Ya-Nan Hao, Hui-Lin Guo,* Lei Tian and Xiaofeng Kang

Received 28th April 2015
Accepted 8th May 2015

DOI: 10.1039/c5ra07745a

www.rsc.org/advances

Graphene quantum dots (GQDs) have attracted tremendous attention due to their unique optical and optoelectronic properties. Doping GQDs with nitrogen atoms can effectively tune their intrinsic properties and exploit new applications in many fields. In this paper, we report a facile yet effective strategy for enhancing the photoluminescent (PL) intensity of nitrogen-doped GQDs (N-GQDs) with enriched pyrrolic-N content using urea as a dopant. The morphology, structure, components, and optical properties of the N-GQDs were characterized systematically. The average diameter of N-GQDs was about 7.5 nm, which was larger than undoped GQDs (~3 nm). Both GQDs and N-GQDs exhibited excitation-independent PL behavior and the PL quantum yields were improved from 9% to 24% after N-doping. Moreover, the PL lifetime decay of GQDs (1.74 ns) and N-GQDs (7.40 ns) can be fitted to a single exponential function very well, indicating that GQDs/or N-GQDs have one single PL origin. Considering the results of Fourier transform infrared spectra and X-ray photoelectron spectra, –COOH groups and pyrrolic-N rings might be feature chromophores of GQDs and N-GQDs, respectively.

1. Introduction

Photoluminescent carbon dots (C-dots) or graphene quantum dots (GQDs) have generated tremendous attention due to their unique chemical, electronic and optical properties.[1–4] Compared with traditional semiconductor quantum dots (QDs) and organic dyes, they have several fascinating merits, such as good biocompatibility, low toxicity, excellent solubility, stable photoluminescence (PL) and tunable band gaps, thus making them promising in photovoltaic devices,[1,2,5] photocatalysts,[6] sensors,[1,7,8] and bioimaging.[1,8,9] The developed routes for GQDs synthesis can be generally divided into "top-down" and "bottom-up" methods. Top-down methods refer to cutting bulk carbon materials into GQDs through physical or chemical approaches, such as ionic liquid assisted grinding,[10] chemical ablation,[11] hydrothermal,[12,13] photo-fenton oxidation,[14] electrochemical oxidation,[5] and oxygen plasma treatment, *etc.* Conversely, bottom-up methods consist of the conversion of suitable organic precursors to GQDs *via* solvothermal treatment,[15–17] microwave,[18] thermal pyrolysis,[19,20] *etc.* Therefore, bottom-up methods have obvious advantages since the composition and physical properties of GQDs can be easily adjusted by careful selecting precursors from diversified organic compounds as well as the carbonization conditions.[19,20]

Heteroatom doping is an effective method to change the electronic density and hence to tune the optical and electrical properties of graphene. Basically, nitrogen atoms doped in graphene exist in three different state, pyridinic-N, graphitic-N and pyrrolic-N. The enhanced catalytic activity of nitrogen doped graphene over undoped graphene is usually attributed to the increased active sites inform of pyridinic-N and/or pyrrolic-N.[21–23] And graphitic-N can improve electrocatalytic activity because of its higher electronic conductivity.[24] Recent study reports that nitrogen induced into GQDs can improve its PL properties.[25] However, the mechanism of nitrogen doping into GQDs and the enhanced PL properties are not clearly understood yet. A summary of the morphologies, nitrogen content and quantum yield of nitrogen doped GQDs and C-dots synthesized *via* typical synthetic routes were listed in Table S1.†

Herein, we reported a facile hydrothermal route to dope nitrogen into GQDs by using urea as N sources. The as-synthesized N-doped GQDs (N-GQDs) were with high pyriolic-N content and their PL quantum yields (QY) were improved from 9% to 24% after doping. The enhanced PL properties were attributed to the formation of the pyrrolic-N in GQDs domains, which substituted the –COOH functional groups at the edges of GQDs. The formation mechanism of the pyrrolic-N rings in N-GQDs was also discussed.

2. Experimental sections

2.1 Preparation of GQDs by pyrolysis of citric acid

The GQDs were synthesized by pyrolyzing citric acid (CA) as described in ref. 20. Briefly, 2 g of CA was put into a 10 mL

Key Laboratory of Synthetic and Natural Functional Molecule Chemistry (Ministry of Education), College of Chemistry and Materials Science, Northwest University, Xi'an 710127, P. R. China. E-mail: hlguo@nwu.edu.cn; Fax: +86 29 81535026; Tel: +86 29 81535026

† Electronic supplementary information (ESI) available. See DOI: 10.1039/c5ra07745a

beaker and heated to 200 °C for 20 min to melt and pyrolyze. The formation of GQDs was indicated by the color of the liquid turning to orange. Then, the liquid was dissolved into 100 mL of 0.25 mol L^{-1} NaOH solutions under continuous and vigorous stirring for 30 min. The color of the solution turned from orange to brown and final faint yellow. The obtained GQD solution was adjusted to pH 9.0 with 0.25 mol L^{-1} NaOH solution.

2.2 Nitrogen doping of GQDs by hydrothermal methods using urea as dopants

In a typical procedure for preparing N-GQDs, 2.5 mL of obtained GQDs solution was mixed with 2.5 mL urea solution with different concentration in a glass vial. After stirring for 30 min, the mixture was transferred to a poly(tetrafluoroethylene)-lined autoclave (30 mL) and heated in the oven for 3 h at 110 °C. After cooling down to room temperature, a homogeneous solution was obtained and filtered using a 0.22 μm cellulose acetate membrane to remove any undissolved materials. The GQDs and N-GQDs samples were obtained by adding water into the solution and centrifuging at 8000 rpm for 10 min. After centrifugation the supernatant was discarded. This process was repeated for three times. Then the below solution was stored at 4 °C for further characterizations of morphology, structure, and optical properties. To characterize the components, the below solution was subsequently purified by dialysis bag (retained molecular weight: 1000 Da) for 7 days.

2.3 General characterization

Elemental analysis was carried out using an organic elemental analyzer (VarioEL III). The Fourier transform infrared (FT-IR) spectra were obtained on a TENSOR 27 FT-IR spectrophotometer (Bruker, Germany). X-ray powder diffraction (XRD) patterns were recorded on a D8 Advance X-ray diffractometer using Cu Kα radiation (Bruker, Germany). X-ray photoelectron spectroscopy (XPS) patterns were measured by a Thermo Scientific K-Alpha spectrometer (Thermo Scientific, America). Transmission electron microscopy (TEM) observations were made on a Tecnai G2F20 S-TWIN transmission electron microscope (FEI, America). Atomic force microscopy (AFM) images were performed in ScanAsyst mode using a MultiMode-8 atomic force microscope (Bruker, Germany). Ultraviolet-visible (UV-Vis) spectroscopy was characterized by a UV-1700 spectrophotometer (Shimazu, Japan). All photoluminescent spectra were accomplished by a FL-4500 spectrophotometer (Hitachi, Japan). The PL decay was carried out by a FLSP920 fluorescence spectrometer (Edinburgh Instruments, UK).

3. Results and discussion

The GQDs were obtained through carbonizing CA at an appropriate degree. During the pyrolysis process of CA, the CA molecules self-assembled *via* the inter-molecular hydrogen bond, and then formed nanocrystalline GQDs with abundant –OH, C═O and –COOH groups on the edges *via* dehydration reaction. N-GQDs were further synthesized by a facile hydrothermal route adopting urea as N sources. Experimental parameters such as feeding concentration and reaction temperature were systematically optimized to obtain brightest PL N-GQDs (Fig. S1 and S2†). The experimental results showed that N-GQDs obtained at 110 °C using 6.5 mol L^{-1} urea possess strongest PL intensity. N-GQDs prepared at the optimized condition were then characterized thoroughly. The element analysis results (shown in Table 1) indicated that the carbon contents of both GQDs and N-GQDs are higher than that of CA. XPS spectra were also performed to analyze the elemental composition and nitrogen bonding configurations in N-GQDs. The calculated atomic percentage of N was 3.99 at%, which accorded with the elemental analysis (3.63 at%). These results indicated that the N atoms were doped into the lattice of GQDs successfully during the hydrothermal procedure in the presence of urea as dopant. The schematic illustration of synthesis procedure of N-GQDs was shown in Fig. 1.

The morphology of the GQDs and N-GQDs was examined by TEM (Fig. 2a and b). The average diameter of GQDs and N-GQDs was found to be about 3 and 7.5 nm, respectively. Furthermore, high-resolution TEM (HRTEM) images showed GQDs and N-GQDs were crystalline with a lattice of ~0.24 nm, which was consistent with the (1120) diffraction planes of sp^2 graphitic carbon, implying that both GQDs and N-GQDs shared similar crystallinity to graphene.[26,27] AFM images of the GQDs (Fig. 3a) showed that the topographic heights were mostly between 0.8 and 1.2 nm. It can be concluded that most of the GQDs were mono-layered or bi-layered with good dispersion. This was similar to the electrochemically synthesized GQDs.[5] After treating with urea at 110 °C, obtained N-GQDs became slightly larger and thicker (Fig. 3b). The topographic heights of N-GQDs were mostly between 0.8 and 1.7 nm, meaning that N-GQDs were mostly in mono-, bi- or tri-layer. Fig. S3† showed the typical XRD profiles for the GQDs and N-GQDs. Just like the GQDs (*ca.* 25.5°), N-GQDs also showed a broad (002) diffraction peak (*ca.* 26.5°), indicating that N-GQDs possessed more compact interlayer spacing (*ca.* 0.336 nm) than GQDs (*ca.* 0.349 nm) due to less oxygen functional groups at the edges.

XPS was employed to determine the elemental compositions, carbon bonding and nitrogen bonding configurations in GQDs and N-GQDs. The XPS survey spectrum of the GQDs and N-GQDs were shown in Fig. 4a. The peaks at ~284.6, 399.2 and 532.6 eV could be signed to the binding energy of C1s, N1s and O1s, respectively. As shown in C1s high-resolution XPS spectra of GQDs (Fig. 4b), there was large number of oxygen functional groups, indicating incomplete carbonization during the pyrolysis of citric acid.[20] Note that C═O was the main oxygen

Table 1 The atomic percent (at%) of GQDs and N-GQDs resulted from elemental analysis and XPS (H was not consideration)

	EA			XPS		
	C (at%)	O (at%, calculated)	N (at%)	C (at%)	O (at%)	N (at%)
GQDs	53.58	46.42	—	55.10	44.90	—
N-GQDs	65.36	31.00	3.63	66.48	29.53	3.99

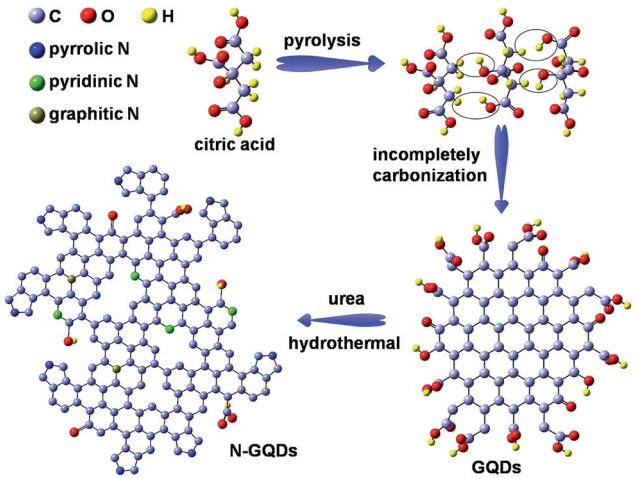

Fig. 1 Schematic illustration of the reaction mechanism of N-GQDs (partly hydrogen atoms are not denoted).

functional groups, which was formed by dehydrating from –OH and –COOH of CA (showed in Fig. 1). As GQDs were treated with urea under hydrothermal condition, the intensity of C=O in N-GQDs became weaker, meanwhile the intensity of O–C=O remain unchanged (Fig. 4c). Moreover, two additional peaks at 285.6 and 287.0 eV corresponding to the C–N and C=N bonds were observed in C1s spectra of N-GQDs, respectively. This strongly indicated that nitrogen was successfully doped into GQDs and N-GQDs formed during the hydrothermal procedure. The high-resolution N1s spectrum of the N-GQDs can be split into three peaks at 398.0 (pyridinic-N), 399.8 (pyrrolic-N) and 401.0 eV (graphitic-N) (Fig. 4d). It can be seen pyrrolic-N was the main component.

FT-IR spectra were also measured to confirm the surface functional groups of GQDs and N-GQDs (Fig. S4†). As shown in the FT-IR spectrum of GQDs, the absorption band at ~3370 and ~1355 cm^{-1} were attributed to the stretching vibration of O–H. The absorption band at ~1579 and ~3082 cm^{-1} can be signed to C=C skeletal vibrations and C–H stretching vibrations in GQDs domains (polycyclic aromatic ring or graphene sheets). The absorption band at ~1680, 1172 and 1074 cm^{-1} was due to the C=O, C–O–C and C–O stretching vibrations, suggesting incomplete carbonization during the pyrolysis of citric acid and the oxygen functional groups remained at the edge of GQDs. The C=O and C–O–C absorption bands were weakened after GQDs been hydrothermally treated with urea. Furthermore, the strong absorption at 3150–3380 cm^{-1} was duo to the N–H stretching vibrations in N-GQDs. In addition, newly appeared absorbing peaks at 1628, 1410 and 1121 cm^{-1} can be attributed to the stretching and bending vibrations of N-related bonds (N–H, C=N and C–N), also indicating that N atoms have been successfully doped into the GQDs. The C=C skeletal vibrations and C–H stretching vibrations in N-GQDs domains were the same as GQDs, indicating the hydrothermal treating has no influence to the lattice structure of GQDs (Fig. 2). These results were also confirmed by XPS spectra.

The as-prepared GQDs and N-GQDs aqueous solution showed faint-yellow and orange color under sunlight, respectively (insets of Fig. 5a and b). Both GQDs and N-GQDs emitted blue photoluminescence when irradiated by a 365 nm UV lamp only N-GQDs with brighter emission. The optical properties of GQDs and N-GQDs were studied and compared by UV/Vis absorption and PL spectroscopy. In the UV/Vis spectra of GQDs (Fig. 5a), a typical absorption peak at 365 nm was attributed to n → π* transition of the C=O bond. This UV/Vis spectrum was similar to that of GQDs prepared through "cutting graphene sheets".[11] For N-GQDs (Fig. 5b), there are two clear absorption bands at 230 nm and 342 nm, which is close to previous reports.[25] These absorption bands are related to π → π* and n → π transition of C=C and C=O bond in the GQDs. Upon excitation with a 365 nm beam, the PL spectrum of the GQDs shows a strong peak at 460 nm with a Stokes shift of 95 nm. Compared with GQDs, both the maximum excitation and maximum emission wavelength (340 and 440 nm) of the N-GQDs showed a blue shift, this may be caused by the relatively strong electron affinity of pyrrolic-N rings in the N-GQDs.

The excitation wavelength dependence of the PL properties such as spectral shift and intensity variation is a fundamental feature observed in carbon-based fluorescent materials.[28] These behaviors may reflect not only the energy gaps distribution induced by size distribution, but also the distribution of various emissive sites on each nanoparticle. Different from traditional carbon nanomaterials, both GQDs and N-GQDs in this work exhibited excitation-independent PL behavior (Fig. 5c and d). In addition, the maximum excitation wavelength of GQDs and N-GQDs were consistent with their maximum absorption wavelength.

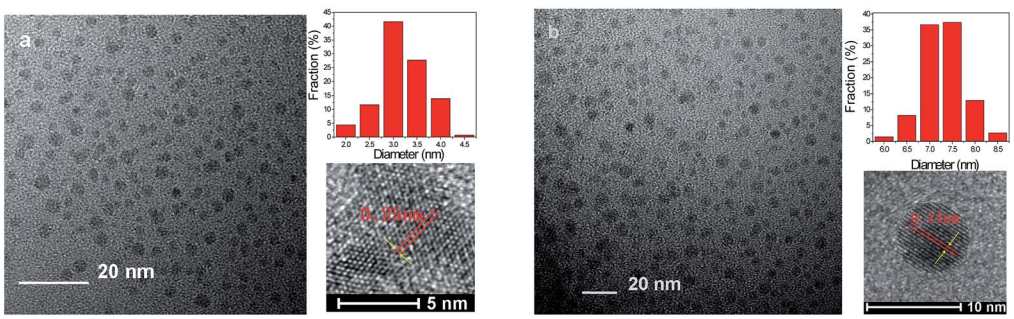

Fig. 2 TEM images of GQDs (a) and N-GQDs (b). Inset images are size distributions (upper) and HRTEM images (under).

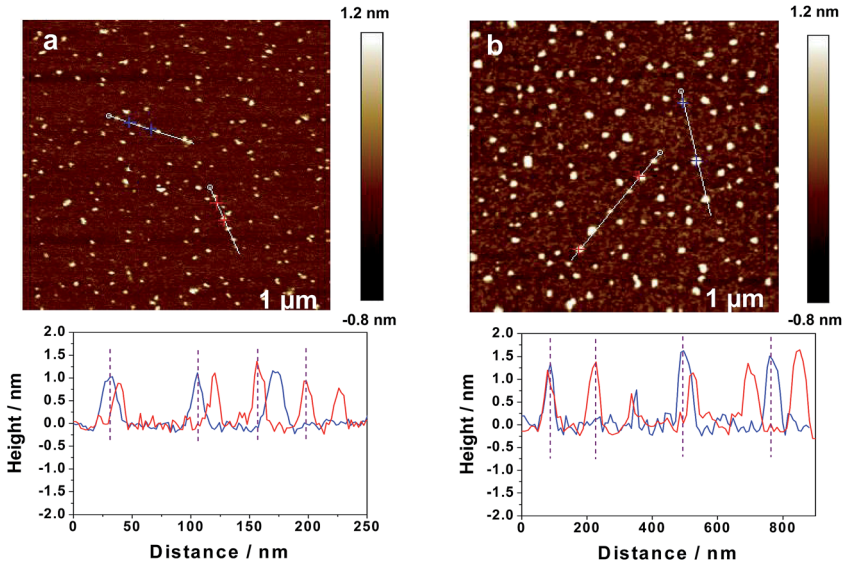

Fig. 3 AFM images of GQDs (a) and N-GQDs (b) on mica sheets. Inset is the height profiles along the line.

The QY was measured using quinine sulfate aqueous (QY = 0.54) as standards. The QY of GQDs was 9%, which was similar to the results of ref. 20. The QY of N-GQDs were almost 2.5 times of that of GQDs. The enhanced PL of N-GQDs, on the one hand, can be attributed to the high pyrrolic-N rings chromophores content in the N-GQDs. On the other hand, less carboxylic and oxygen-containing groups which were acting as the non-radiative electron–hole recombination centers were also leading to the efficient emission.

The PL decay profiles of GQDs and N-GQDs are shown in Fig. 5e and f. The decay were recorded as at 460 nm emission for the GQDs and 440 nm for N-GQDs, which was excited under 360 and 340 nm respectively at room temperature by a time correlated single photon counting technique. The parameters generated from iterative reconvolution of the decay with the instrument response function. The PL lifetime decay of GQDs and N-GQDs were fitted to a single exponential function. It should be noted that PL lifetime decay of N-GQDs (7.40 ns) was different from that of GQDs (1.74 ns), indicating that N-GQDs had a discrepant PL origin from that of GQDs. Remarkably, this results was according with that obtained from the sample treated by dialyzing (7.83 ns for N-GQDs, 1.65 ns for GQD,

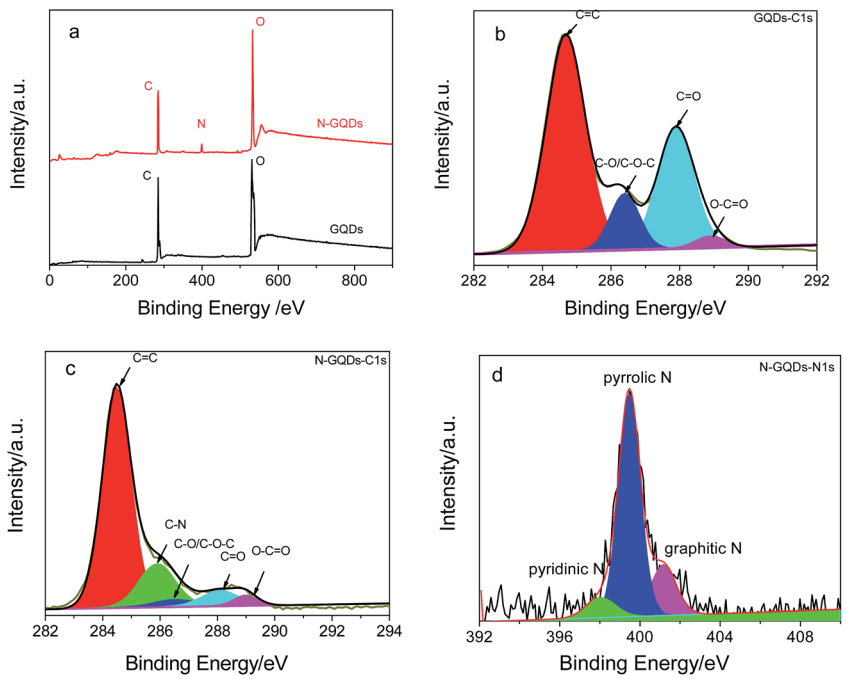

Fig. 4 (a) XPS survey spectrum of GQDs and N-GQDs. (b) High resolution C1s XPS spectra of GQDs. (c) High resolution C1s XPS spectra of N-GQDs. (d) High resolution XPS of N1s of N-GQDs.

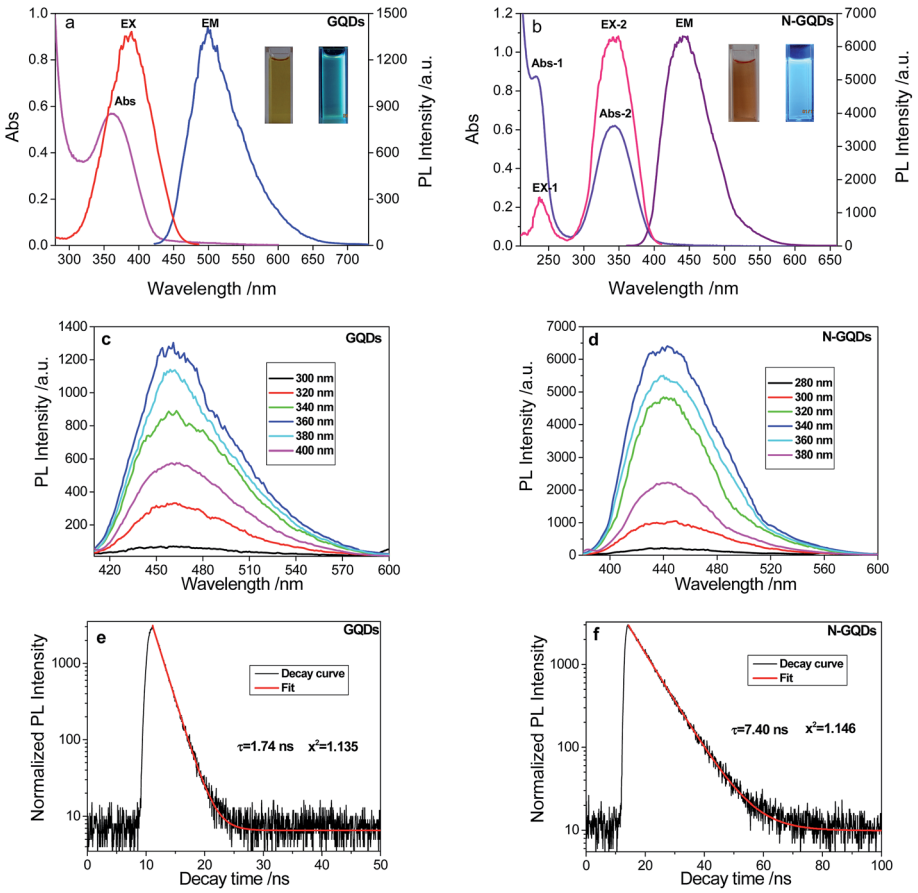

Fig. 5 The spectra properties of GQDs and N-GQDs. The UV-Vis absorption, PL emission and PL excitation spectra of GQDs (a) and N-GQDs (b). The inset shows photographs of an aqueous solution of GQDs taken under visible-light (left) and UV irradiation at 365 nm (right). The PL spectra of GQDs (c) and N-GQDs (d) under different excitation wavelengths. PL decay of GQDs (e) and N-GQDs (f).

Fig. S5†). Thus, the main reasons for high PL quantum yields can be attributed to the N-doping.

The effect of pH on the PL intensity of GQDs and N-GQDs was also investigated (Fig. S6†). The experimental results showed that the PL emission of the GQDs was pH-dependent, indicating that the PL origin of GQDs was surface dependent. This can be attributed to the –COOH groups at the edge of GQDs. However, N-GQDs exhibited less pH-dependent, showing their surface functional group was less sensitive to pH changes. Combined with the results of FT-IR and XPS, the enhanced PL intensity of N-GQDs can be ascribed to the formation of pyrrolic-N rings in the GQDs domains. Nitrogen atoms in pyrrolic-N rings were sp^2 hybridization. They shared their lone electron pairs to π plane conjugate system of the GQDs domains, forming an electron-rich density distribution, which played important roles in PL emission of N-GQDs. In addition, the suspension of GQDs and N-GQDs also showed extra-high stability even after being kept for months in air at room temperature; it still exhibited a transparent appearance and strong PL (Fig. S7†), this offers another advantage for its future applications.

Qu *et al.* reported a one-step microwave synthesis of C-dots (N/C atomic ratio 0.429) using CA and urea as raw materials.[29] In order to eliminate the interference of the reaction products caused by CA remain reacting with urea during the hydrothermal process to induce nitrogen into GQDs. The mixture solution of CA and urea was adjusted to different pH values using 0.25 mol L^{-1} NaOH and then heated at 110 °C for 3 h (Fig. S8†). The experimental results showed that the PL intensity decreased as the pH values changed from 1.0 to 9.0. Almost no PL was appeared at pH 9.0, indicting no PL C-dots was produced at this condition.

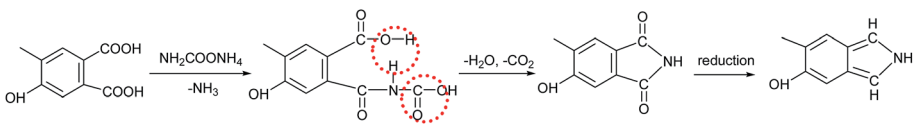

Fig. 6 Possible formation process of pyrrolic-N in GQDs.

Compared with the GQDs-U (1 step to obtain) in ref. 25, N-GQDs as-synthesized from 2 steps in our experiments has the same UV-Vis and PL spectra. N-GQDs as-synthesized in our experiments has lower QY (24%) than that of GQDs-U (QY 78%, Table S1;† N/C atomic ratio ~0.2, Fig. S4 in ref. 25). This can be attributed the lower N/C atomic ratio of the N-GQDs. And the PL origin of the as-synthesized N-GQDs can be regard as the same as that of GQDs-U-4 (τ_{ave} = 8 ns) since they have almost the same PL lifetime.

The mechanism of nitrogen doping into GQDs can be described as: when the mixture solution of GQDs and urea were heated, urea firstly hydrolyzed to form ammonium carbamate.[30] Subsequently, ammonium carbamates reacted with carboxylic groups at the edge of GQDs to form amide groups. Meanwhile, the carboxylic groups of ammonium carbamate were removed to release CO_2. Then, the amides reacted with neighbor carboxylic groups of GQDs and formed pyrrolic-N rings through the intramolecular dehydrolysis.[25] The contents of oxygen functional groups (C=O bondings) in N-GQDs was decreased because of the reduction of urea. The schematic illustration of the formation of pyrrolic-N rings was shown in Fig. 6.

4. Conclusion

A facile yet effective strategy for enhancing photoluminescent (PL) intensity of N-GQDs with enriched pyrrolic-N content using urea as dopants was reported. The average diameter of N-GQDs was about 7.5 nm, which was larger than that of GQDs (~3 nm). The optical research results showed that N-GQDs exhibited excitation-independent PL behavior and the PL QY was 24%. Moreover, the PL lifetime decay N-GQDs (7.4 ns) was very well fitted to a single exponential function. Combined with the results of FT-IR and XPS, it can be concluded that pyrrolic-N rings in GQDs domains play an important role in PL emission.

Acknowledgements

This work was supported by the National Natural Science Foundation of China (21175105, 21375104), the Natural Science Foundation of Shaanxi Province of China (2014JM2042), and State Key Laboratory of Analytical Chemistry for Life Science (SKLACLS1210) and the Scientific Research Foundation of Education Bureau of Shaanxi Province of China (14JK1728).

References

1 J. Shen, Y. Zhu, X. Yang and C. Li, *Chem. Commun.*, 2012, **48**, 3686–3699.
2 Z. Zhang, J. Zhang, N. Chen and L. Qu, *Energy Environ. Sci.*, 2012, **5**, 8869–8890.
3 S. Zhu, S. Tang, J. Zhang and B. Yang, *Chem. Commun.*, 2012, **48**, 4527–4539.
4 L. Li, G. Wu, G. Yang, J. Peng, J. Zhao and J.-J. Zhu, *Nanoscale*, 2013, **5**, 4015–4039.
5 Y. Li, Y. Hu, Y. Zhao, G. Shi, L. Deng, Y. Hou and L. Qu, *Adv. Mater.*, 2011, **23**, 776–780.
6 S. Zhuo, M. Shao and S.-T. Lee, *ACS Nano*, 2012, **6**, 1059–1064.
7 H. Razmi and R. Mohammad-Rezaei, *Biosens. Bioelectron.*, 2013, **41**, 498–504.
8 S. Zhu, Q. Meng, L. Wang, J. Zhang, Y. Song, H. Jin, K. Zhang, H. Sun, H. Wang and B. Yang, *Angew. Chem., Int. Ed.*, 2013, **52**(14), 3953–3957.
9 J. Peng, W. Gao, B. K. Gupta, Z. Liu, R. Romero-Aburto, L. Ge, L. Song, L. B. Alemany, X. Zhan, G. Gao, S. A. Vithayathil, B. A. Kaipparettu, A. A. Marti, T. Hayashi, J.-J. Zhu and P. M. Ajayan, *Nano Lett.*, 2012, **12**, 844–849.
10 N. G. Shang, P. Papakonstantinou, S. Sharma, G. Lubarsky, M. Li, D. W. McNeill, A. J. Quinn, W. Zhou and R. Blackley, *Chem. Commun.*, 2012, **48**, 1877–1879.
11 D. Pan, J. Zhang, Z. Li and M. Wu, *Adv. Mater.*, 2010, **22**, 734–738.
12 S. Kim, S. W. Hwang, M.-K. Kim, D. Y. Shin, D. H. Shin, C. O. Kim, S. B. Yang, J. H. Park, E. Hwang, S.-H. Choi, G. Ko, S. Sim, C. Sone, H. J. Choi, S. Bae and B. H. Hong, *ACS Nano*, 2012, **6**, 8203–8208.
13 D. Y. Pan, L. Guo, J. C. Zhang, C. Xi, Q. Xue, H. Huang, J. H. Li, Z. W. Zhang, W. J. Yu, Z. W. Chen, Z. Li and M. H. Wu, *J. Mater. Chem.*, 2012, **22**, 3314–3318.
14 X. Zhou, Y. Zhang, C. Wang, X. Wu, Y. Yang, B. Zheng, H. Wu, S. Guo and J. Zhang, *ACS Nano*, 2012, **6**, 6592–6599.
15 D. Deng, X. Pan, L. Yu, Y. Cui, Y. Jiang, J. Qi, W.-X. Li, Q. Fu, X. Ma, Q. Xue, G. Sun and X. Bao, *Chem. Mater.*, 2011, **23**, 1188–1193.
16 M. Xu, Z. Li, X. Zhu, N. Hu, H. Wei, Z. Yang and Y. Zhang, *Nano Biomed. Eng.*, 2013, **5**, 65–71.
17 Y. Feng, J. Zhao, X. Yan, F. Tang and Q. Xue, *Carbon*, 2014, **66**, 334–339.
18 L.-L. Li, J. Ji, R. Fei, C.-Z. Wang, Q. Lu, J.-R. Zhang, L.-P. Jiang and J.-J. Zhu, *Adv. Funct. Mater.*, 2012, **22**, 2971–2979.
19 R. Liu, D. Wu, X. Feng and K. Müllen, *J. Am. Chem. Soc.*, 2011, **133**, 15221–15223.
20 Y. Dong, J. Shao, C. Chen, H. Li, R. Wang, Y. Chi, X. Lin and G. Chen, *Carbon*, 2012, **50**, 4738–4743.
21 P. H. Matter, L. Zhang and U. S. Ozkan, *J. Catal.*, 2006, **239**, 83–96.
22 S. Maldonado and K. J. Stevenson, *J. Phys. Chem. B*, 2005, **109**, 4707–4716.
23 Y. Li, Y. Zhao, H. Cheng, Y. Hu, G. Shi, L. Dai and L. Qu, *J. Am. Chem. Soc.*, 2011, **134**, 15–18.
24 H. Niwa, K. Horiba, Y. Harada, M. Oshima, T. Ikeda, K. Terakura, J.-I. Ozaki and S. Miyata, *J. Power Sources*, 2009, **187**, 93–97.
25 D. Qu, M. Zheng, L. Zhang, H. Zhao, Z. Xie, X. Jing, R. E. Haddad, H. Fan and Z. Sun, *Sci. Rep.*, 2014, **4**, 1–9.
26 D. Qu, M. Zheng, P. Du, Y. Zhou, L. Zhang, D. Li, H. Tan, Z. Zhao, Z. Xie and Z. Sun, *Nanoscale*, 2013, **5**, 12272–12277.
27 X. T. Zheng, A. Than, A. Ananthanaraya, D.-H. Kim and P. Chen, *ACS Nano*, 2013, **7**, 6278–6286.
28 Y. Wang, L. Zhang, R.-P. Liang, J.-M. Bai and J.-D. Qiu, *Anal. Chem.*, 2013, **85**, 9148–9155.
29 S. Qu, X. Wang, Q. Lu, X. Liu and L. Wang, *Angew. Chem.*, 2012, **124**, 12381–12384.
30 K. G. Clark, V. L. Gaddy and C. E. Rist, *Ind. Eng. Chem.*, 1933, **25**, 1092–1096.